Effect of Glycosylation on the Function of a Soluble, Recombinant Form of the Transferrin Receptor†

Shaina L. Byrne,‡ Rachael Leverence,§ Joshua S. Klein,|| Anthony M. Giannetti,||,⊥ Valerie C. Smith,# Ross T. A. MacGillivray,# Igor A. Kaltashov,§ and Anne B. Mason*,‡

Department of Biochemistry, University of Vermont College of Medicine, Burlington, Vermont 05405-0068, Department of Chemistry, University of Massachusetts at Amherst, Amherst, Massachusetts 01003, Graduate Option in Biochemistry and Molecular Biophysics, California Institute of Technology, Pasadena, California 91125, and Department of Biochemistry and Molecular Biology and Centre for Blood Research, University of British Columbia, Vancouver, British Columbia V6T 1Z3, Canada

Received January 12, 2006; Revised Manuscript Received March 23, 2006

ABSTRACT: Production of the soluble portion of the transferrin receptor (sTFR) by baby hamster kidney (BHK) cells is described, and the effect of glycosylation on the biological function of sTFR is evaluated for the first time. The sTFR (residues 121−760) has three N-linked glycosylation sites (Asn251, Asn317, and Asn727). Although fully glycosylated sTFR is secreted into the tissue culture medium (∼40 mg/L), no nonglycosylated sTFR could be produced, suggesting that carbohydrate is critical to the folding, stability, and/or secretion of the receptor. Mutants in which glycosylation at positions 251 and 727 (N251D and N727D) is eliminated are well expressed, whereas production of the N317D mutant is poor. Analysis by electrospray ionization mass spectrometry confirms dimerization of the sTFR and the absence of the carbohydrate at the single site in each mutant. The effect of glycosylation on binding to diferric human transferrin (Fe_2 hTF), an authentic monoferric hTF with iron in the C-lobe (designated Fe_C hTF), and a mutant (designated Mut-Fe_C hTF that features a 30-fold slower iron release rate) was determined by surface plasmon resonance; a small (∼20%) but consistent difference is noted for the binding of Fe_C hTF and the Mut-Fe_C hTF to the sTFR N317D mutant. The rate of iron release from Fe_C hTF and Mut-Fe_C hTF in complex with the sTFR and the sTFR mutants at pH 5.6 reveals that only the N317D mutant has a significant effect. The carbohydrate at position 317 lies close to a region of the TFR previously shown to interact with hTF.

Transferrin (TF) is a bilobal metal binding protein that transports iron to cells. The N- and C-lobes of human TF (hTF)[1] are homologous globular domains that can each bind one atom of ferric iron (Fe^{3+}) in a cleft formed by two subdomains. The iron is coordinated by two tyrosines, a histidine, an aspartic acid residue, and two oxygen atoms from the synergistic carbonate anion, which is anchored by a conserved arginine residue (*1*). Since ferric iron is insoluble in aqueous solution at physiological pH, binding to hTF is an absolute requirement for delivery of iron to cells. Diferric hTF (Fe_2 hTF) in the circulation preferentially binds to the extracellular portion of the transferrin receptor (TFR) on the cell surface at neutral pH (∼7.4). Monoferric hTF binds to the TFR an order of magnitude less tightly than Fe_2 hTF, and apo-hTF does not effectively compete with diferric or the two monoferric hTF species for binding to the TFR (*2*, *3*). The Fe_2 hTF/TFR complex is endocytosed into a clathrin-coated pit forming an endocytic vesicle. The coat disassembles as the endocytic vesicles fuse within the cell. The pH within the endosome is lowered to pH ∼5.6 by a mechanism involving a proton pump which leads to iron release (*4*, *5*). Although all of the details related to the release

† This work was supported by USPHS Grants R01 DK21739 (A.B.M.), R01 GM061666 (I.A.K.), and R01 DK60770 (P.J.B.) and the Howard Hughes Medical Institute (to Pamela J. Bjorkman). S.L.B. was supported by a predoctoral fellowship from the NRSA Hemostasis & Thrombosis Training Grant. J.S.K. was supported by biology funds from the Lawrence Ferguson Endowment.

* Correspondence should be addressed to this author. Phone: (802) 656-0343. Fax: (802) 656-8220. E-mail: anne.mason@uvm.edu.

‡ University of Vermont College of Medicine.

§ University of Massachusetts at Amherst.

|| California Institute ofTechnology.

⊥ Current address: Roche Palo Alto, LLC, Palo Alto, CA 94043.

University of British Columbia.

[1] Abbreviations: WT, wild type; hTF, human serum transferrin that is glycosylated; hTF-NG, human serum transferrin that is nonglycosylated; Fe_2 hTF, diferric human serum transferrin; N-His hTF-NG, recombinant nonglycosylated human serum transferrin with an N-terminal hexahistidine tag and a factor Xa cleavage site attached to the amino terminus of the protein; Fe_C hTF, N-His Y95F/Y188F hTF-NG monoferric hTF with iron in the C-lobe; Mut-Fe_C hTF, slowly releasing C-lobe mutant (N-His Y95F/Y188F/R632N/D634N hTF-NG); TFR, transferrin receptor 1; sTFR, recombinant soluble portion of transferrin receptor 1 with an N-terminal hexahistidine tag, a factor Xa cleavage site, and residues 121−760 of the TFR; N251D, N317D, and N727D, sTFR mutants containing Asn → Asp mutations at the indicated positions; DMEM-F12, Dulbecco's modified Eagle's medium−Ham F-12 nutrient mixture; BHK cells, baby hamster kidney cells; CHO cells, Chinese hamster ovary cells; UG, Ultroser G; FBS, fetal bovine serum; BSA, bovine serum albumin; HRP, horseradish peroxidase; TMB, 3,3′,5,5′-tetramethylbenzidine; EDTA, ethylenediaminetetracetic acid; MES, morpholinoethanesulfonic acid; Ni-NTA, nickel nitrilotriacetic acid; DMT-1, divalent metal transporter; ER, endoplasmic reticulum; SPR, surface plasmon resonance; NaN_3, sodium azide; ESI MS, electrospray ionization mass spectrometry.

10.1021/bi0600695 CCC: $33.50
Published on Web 05/05/2006

of iron are not clear, it appears that ferric iron may be reduced by a newly described ferrireductase (*6*), and the resulting ferrous iron crosses the endosomal membrane for use by the cell in a process involving the divalent metal transporter, DMT-1 (*7*). Critical to the cycle, apo-hTF remains bound to TFR at acidic pH and is transported back to the plasma membrane surface where it is released to bind more ferric iron. The complete process of iron delivery takes only 2−3 min (*8*).

The ubiquitous TFR (also known as TFR-1) is an inducible 760 amino acid, membrane-bound protein. A constitutively expressed TFR, known as TFR-2, has also been identified (*9*). TFR is initially synthesized as an 86 kDa protein that dimerizes shortly after synthesis forming a homodimer held together by two intermolecular disulfide bonds (Cys89 and Cys98) (*10*, *11*). After exiting the endoplasmic reticulum (ER), N-linked glycosylation occurs at three asparagine residues (Asn251, Asn317, and Asn727) and one O-linked threonine residue (Thr104), yielding a protein with a mass of ∼190 kDa (*10*, *12*). The predicted TFR primary amino acid sequence (*13*, *14*) led to the identification of three distinct regions: a globular extracellular portion which binds hTF (residues 90−760), a hydrophobic membrane-spanning segment (residues 62−89), and the remaining 61 residues which lie within the cytoplasm and contain signaling motifs (*15*). Residues 89−126 of the TFR comprise a stalk separating the extracellular domain from the transmembrane domain.

The crystal structure of a recombinant form of the soluble TFR (sTFR, comprised of residues 121−760) expressed by Chinese hamster ovary cells was determined by Lawrence et al. (*11*). The structure revealed that the extracellular portion of the TFR is comprised of three subdomains: a protease-like domain (resembling amino- and carboxypeptidases), an apical domain, and a helical domain (Figure 1A). Experimentally, the sTFR is easier to work with since it remains soluble in the absence of the detergent required to maintain the full-length TFR in solution. The development of a robust baculovirus/insect cell expression system by Drs. Snow and Bjorkman (including the attachment of a hexa-His tag to the N-terminus for ease of purification) has made recombinant sTFR available to the research community (*16*−*19*). This expression system also allows production of site-directed mutants to determine the role of specific amino acid residues involved in binding of hTF. Parenthetically, the HFE protein also binds TFR. This protein is defective in individuals suffering from hereditary hemochromatosis in which there is an increase in the intestinal absorption of iron leading to excessive iron stores and iron overload (*20*). Significantly, hTF and HFE compete with each other for binding to TFR, implying that they share recognition sequences on the TFR (*20*, *21*). The availability of the crystal structure of the HFE/sTFR complex identified the amino acid residues involved in binding of HFE to sTFR and, thereby, also provided information with regard to potential binding region(s) of hTF (*22*). An earlier study (*23*) had identified a conserved Arg-Gly-Asp sequence at residues 646−648 in the TFR which is critical to hTF binding and accounts at least in part for the high-affinity interaction. Extensive mutagenesis and binding studies by Giannetti et al. (*17*) identified other specific residues in the TFR crucial to the binding of HFE and of hTF. Importantly, this work showed differential

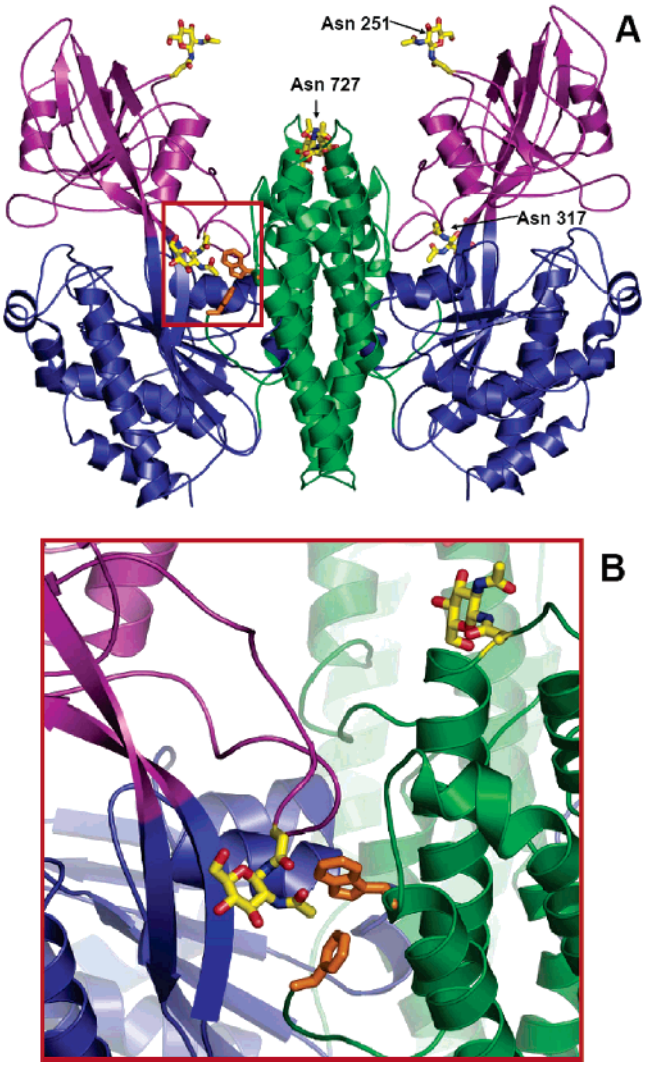

FIGURE 1: Crystal structure of sTFR (PDB code 1CX8) adapted from Lawrence et al. (*11*). (A) Asn-linked glycosylation sites are labeled on one monomer and shown in yellow. The extracellular portion of the TFR is comprised of three subdomains: a protease-like domain resembling amino- and carboxypeptidases (residues 121−188 and 384−606 shown in blue), an apical domain (residues 189−383, purple), and a helical domain (residues 607−760, green). The hydrophobic patch residues Trp641 and Phe760 are in orange. (B) Close-up of the region indicated in the red box in (A) to highlight the residues and the proximity of Asn317 (yellow) to the hydrophobic patch residues Trp641 and Phe760 (orange) involved in hTF binding. The residue in the upper right-hand corner is Asn727.

binding affinities of the sTFR for apo-hTF and Fe_2 hTF as a function of pH. In particular, two TFR residues (Trp641 and Phe760) reside in the helical domain and form a hydrophobic patch (see below).

Earlier work of Aisen and colleagues (initially utilizing TFR isolated from placenta and more recently the recombinant sTFR) was pivotal in establishing the crucial role of the TFR in facilitating iron release from hTF at the appropriate time and place (*24*−*27*). This group established techniques that unequivocally showed that TFR inhibits iron release from hTF at pH 7.4 and accelerates it at the putative endosomal pH of ∼5.6. More recently, other approaches to map the TFR and hTF interface have been reported (*28*, *29*), complementing the site-directed mutagenesis work from the Bjorkman laboratory mentioned above (*17*). The differential

effect of radiation damage on hTF (or the C-lobe of hTF) and the TFR individually compared to the hTF/TFR complex has been determined, providing a "footprint" that identifies residues in each that are protected by complex formation (*28*). A second approach involved construction of an atomic model obtained by fitting crystal structures of the human N-lobe and rabbit C-lobe into a map of the sTFR (*29*). This cryo-EM study has identified residues in both the sTFR and hTF involved in complex formation. It is proposed that the C-lobe makes contact through the C-I subdomain with the helical region of the sTFR, allowing the C-II subdomain to move freely. It is further suggested that the N-lobe binds TFR through both subdomains in contact with the helical and the protease-like domain on the underside of the TFR, placing the N-lobe between the TFR and the membrane.

Recent experiments provide additional insight into the importance of Trp641 and Phe760 from sTFR in the pH-dependent release of iron from hTF (*30*). The double mutant W641A/F760A sTFR was found to bind Fe_2 hTF with an affinity close to that found for wild-type (WT) sTFR at pH 7.4, 6.3, and 5.6. In contrast, apo-hTF binds this mutant sTFR with a 400−1000-fold lower affinity at pH 6.3 and 5.6, respectively, compared to WT sTFR. Furthermore, the double mutant actually slows iron release from the C-lobe of monoferric hTF by a factor of 2.

As mentioned, TFR has three N-linked glycosylation sites. As shown in Figure 1A, Asn727 is found in the helical domain while Asn 251 and 317 both reside in the apical domain. Of interest is the observation that Asn317 appears to reside close to the hydrophobic patch of the sTFR described above (Figure 1B). Extensive work from the laboratories of Enns, Hunt, and colleagues has established the importance of glycosylation in the proper folding, transport, and insertion of full-length TFR into the plasma membrane (*10*, *31*−*36*). Protein structure and stability, intracellular trafficking, and localization as well as protection from proteolysis and enhanced solubility are known to be influenced by attachment of carbohydrate (ref *37* and references cited therein). Additionally, different glycoforms have different effects on these properties (*38*).

In the current study we report the development of an expression system using baby hamster kidney (BHK) cells to synthesize and secrete a His-tagged soluble TFR construct similar to that produced previously in insect cells (*18*). The rationale for producing this construct in a different expression system is threefold: (1) to explore the possibility of obtaining higher yields in a system in which we have extensive experience; (2) to provide a different target for crystallization studies since the glycosylation composition is likely to vary in the two expression systems; and (3) to allow us to pursue further mutagenesis studies. We have established a competitive immunoassay to measure the expression levels of the WT and mutant sTFR permitting the optimization of our expression system. Additionally, we have produced mutants in which each of the three asparagine residues have been converted to aspartic acid to prevent glycosylation, and we have analyzed the composition of these constructs by mass spectrometry. We report the binding constants for each of the sTFR glycosylation mutants by using surface plasmon resonance (SPR). We also report the rate constants for the release of iron from the C-lobe of a monoferric hTF (Fe_C hTF) and a mutant of Fe_C hTF (designated Mut-Fe_C hTF) bound to each sTFR construct. In the case of the Fe_C hTF/sTFR complex we are using a newly developed stopped-flow procedure which provides these rates with greater precision. For the first time, the effect of glycosylation on the biological function of the soluble TFR is revealed.

MATERIALS AND METHODS

Materials. Dulbecco's modified Eagle's medium−Ham F-12 nutrient mixture (DMEM-F12), antibiotic−antimycotic solution (100×), and trypsin were from the GIBCO-BRL Life Technologies Division of Invitrogen. The *Escherichia coli* strain MACHI was also purchased from Invitrogen. Fetal bovine serum (FBS) was obtained from Atlanta Biologicals (Norcross, GA) and was tested prior to use to ensure adequate growth of BHK cells. Ultroser G (UG) is a serum replacement from Pall BioSepra (Cergy, France). The QuikChange mutagenesis kit and pBluescriptII were from Strategene. Ni-NTA resin and the Qiaquick nucleotide removal kit were from Qiagen. The Klenow fragment and buffer were from New England Biolabs. Corning expanded surface roller bottles and Dynatech Immunolon 4 Removawells were obtained from Fisher Scientific. The Hi-Prep 26/60 Sephacryl S-300HR column was from Amersham Pharmacia. Methotrexate from Bedford Laboratories was purchased at a local hospital pharmacy and used for selection of plasmid-containing BHK cells. Centricon 30 microconcentrators, YM-30 ultrafiltration membranes, and spiral cartridge concentrator (CH2PRS) fitted with an S1Y10 cartridge were from Millipore/Amicon. Bovine serum albumin (BSA) was from Sigma. Rabbit anti-mouse immunoglobulin G was from Southern Biological Associates. Immunopure NHS-LC-biotin and immunopure avidin−horseradish peroxidase were from Pierce. The TMB Microwell peroxidase substrate system was obtained from Kirkegaard and Perry Laboratories (Gaithersburg, MD). Human serum TF was purchased from Intergen (Purchase, NY) or from Sigma. The A4A6 monoclonal antibody to TFR was a generous gift from the laboratory of Dr. James Cook at the University of Kansas Medical Center. All other chemicals and reagents were of analytical grade or better.

Preparation of Plasmids. A full-length human TFR cDNA clone was kindly provided by Dr. Caroline Enns (Department of Cell and Developmental Biology, Oregon Health & Science University). The cDNA was engineered for the expression of sTFR that contained the signal peptide of hTF, four amino acids (V-P-D-K) from the N-terminus of hTF, six histidine residues, a factor Xa cleavage site, and the N-terminal region of the TFR beginning at residue 121. A double-stranded synthetic oligonucleotide was formed by hybridizing two overlapping oligonucleotides (Table 1, oligos 1 and 2); aliquots (10 μL of a 2 μg/μL solution) of both oligonucleotides were diluted with 20 μL of Klenow buffer and incubated at 85.0 °C for 30 min, cooled to room temperature, and placed at 4 °C overnight. The overhanging ends were filled in by using the Klenow fragment of *E. coli* DNA polymerase and 10 mM dNTPs. This double-stranded oligonucleotide was purified using the Qiaquick nucleotide removal kit and was used as the forward primer in a PCR reaction together with an internal TFR primer (Table 1, oligo 3) containing an *Mfe*I restriction site. The resulting PCR fragment (coding for a hexa-His-tagged N-terminal sequence and amino acid residues 121−275 of the TFR) was cleaved

Table 1: Sequences of the Mutagenic Primers Used in This Study

oligo 1: 5′ -AAA CCC GGG AAG ATG AGG CTC GCC GTG GGA GCC CTG CTG GTC TGC GCC GTC CTA GGG CTG TGT CTG GCT GTC CCT 3′
oligo 2: 5′ TCA GGT CAT CCC AAT ATA AGC GCC TTC CCT CGA TGA ATT CAT GAT GAT GAT GAT GAT GTT TAT CAG GGA CAG CCA GAC A 3′
oligo 3:[a] 5′ CAC ACC AAT TGC ATT TAA 3′
N251D:[b] 5′ TA TAC ACT CCT GTG **G**AT GGA TCT ATA GTG ATT GTC AGA GC 3′
N317D:[b] 5′ A TTC CCT TCC TTC **G**AT CAC ACT CAG TTT CCA CCA TCT CGG 3′
N727D:[b] 5′ CAA AAT AAC GGT GCT TTT **G**AT GAA ACG CTG TTC AGA AAC C 3′

[a] The underlined region represents the *Mfe*I restriction site used in a subsequent cloning step. [b] The mutagenic base is represented by the bold, underlined base.

with *Sma*I and *Mfe*I, made blunt ended with Klenow fragment and 10 mM dNTPs, and cloned into the *Sma*I site of pBluescriptII (pBSSK). Both the full-length TFR construct and the cloned PCR fragment were digested with *Mfe*I and *Xba*I, and the appropriate fragments were isolated by gel electrophoresis and Qiaquick gel extraction purification. The two fragments containing *Mfe*I and *Xba*I overhanging ends were ligated overnight at 14 °C and used to transform *E. coli* strain MACHI. Subsequent DNA sequence analysis revealed a clone with a plasmid containing the correct predicted N-terminal sequence of TFR. The cDNA from the pBSSK clone was cleaved with *Sma*I and *Xba*I; the overhang created by *Xba*I was made blunt using Klenow fragment and 10 mM dNTPs, purified using the Qiaquick gel extraction kit, and ligated into the *Sma*I site of pNUT.

The three N-linked glycosylation sites at positions 251, 317, and 727 in the sTFR in the pNUT vector were mutated from Asn to Asp using the QuikChange mutagenesis procedure (*39*, *40*). The mutagenic primers are shown in Table 1. To make the sTFR mutant lacking all three glycosylation sites, the N251D sTFR mutant in the pNUT vector was mutated at position 317 to create a double mutant which was used as the template for the final mutation at position 727. In all cases, the presence of the correct mutation and the absence of unwanted mutations were confirmed by DNA sequence analysis. Transfection of BHK cells and selection with methotrexate were carried out as described in detail previously (*40*).

The expression and purification of sTFR in the baculovirus/insect cell system at the California Institute of Technology have been described in detail previously (*41*). Briefly, the gene encoding residues 121−760 of the TFR was fused 3′ to a gene segment encoding the hydrophobic leader peptide from the baculovirus protein gp67 with a hexa-His tag and a factor Xa cleavage site.

sTFR Production. The protocol for transferring the transfected BHK cells into expanded surface roller bottles has been described previously (*39*, *40*, *42*). In each production run, the first three batches contain DMEM-F12−10% FBS and were not saved. The subsequent batches (4−7) contained DMEM-F12 with 1% UG + 1 mM butyric acid replacing the FBS and were pooled following addition of 0.02% sodium azide (NaN_3) and stored at 4 °C until purification.

sTFR Assay. The amount of sTFR in the tissue culture medium and at various stages of purification was determined using a specific monoclonal antibody to the TFR in a competitive solid-phase immunoassay as previously described in detail for hTF (*39*). In the assay, a constant amount of biotinylated N-His sTFR was mixed with unlabeled N-His sTFR standards ranging from 16 to 400 ng/well and varying amounts of sample and added to each well in duplicate. The amount of sTFR in each sample was determined by comparison with the standard curve generated from the unlabeled standards.

sTFR Purification. The purification of N-His sTFR followed a protocol developed for N-His hTF (*40*) in which the pooled batches were concentrated and exchanged into 5 mM Tris, pH 8.0, containing 0.02% NaN_3 using a Millipore spiral wound membrane concentrator fitted with an S1Y10 cartridge. Each sample was filtered through a 0.22 μm Sterivex filter, and Qiagen start buffer (5×) was added to yield a final concentration of 50 mM Tris, pH 7.5, containing 300 mM NaCl, 20 mM imidazole, 10% glycerol, and 0.05% NaN_3. The sample was then loaded onto a Ni-NTA column (1 × 10 cm) at a flow rate of 2 mL/min. The column was attached to a BioCad Sprint system (Applied Biosystems) to allow continuous monitoring of the absorbance at 280 nm, the conductivity, and the pH. After being loaded onto the column and washed with start buffer (1×) until the $A_{280} < 0.1$, the N-His sTFR was displaced with elution buffer (start buffer containing 250 mM imidazole). Peak fractions were pooled, reduced using YM30 Centricon microconcentrators to less than 2 mL, filtered through a 0.22 μm Millex syringe filter, and loaded onto a Sephacryl S300HR 26/60 column equilibrated and run in 0.1 M NH_4HCO_3 at a flow rate of 1.5 mL/min. Following pooling of appropriate fractions, aliquots were analyzed on a 10% SDS−PAGE gel to verify purity. An identical procedure was used to purify the N-His sTFR obtained from The California Institute of Technology (*15*−*18*). In this case, the recombinant sTFR was secreted by insect cells into the medium which was shipped to Vermont.

The sTFR contains 11 tryptophans, 24 tyrosines, and 2 cystines, yielding a calculated millimolar extinction coefficient of 96.51 (*43*). The calculated mass of the nonglycosylated sTFR (residues 121−760) is 71726 Da, to which is added 440 Da for the V-P-D-K sequence, 823 Da for the hexa-His tag, and 456 Da for the factor Xa cleavage sequence for a total mass of 73445 Da. From the mass spectrometry results, the monomer mass of the glycosylated TFR is 79760 Da. The concentration (in milligrams per milliliter) for sTFR can be determined from the A_{280} by dividing by 1.21. The production and purification of the recombinant hTF samples, Fe_C hTF and Mut-Fe_C hTF, have been described in detail elsewhere (*40*, *44*).

Mass Spectrometry. Electrospray ionization mass spectra of all protein samples were obtained under nondenaturing conditions using a JMS-700 MStation (JEOL, Tokyo, Japan) two-sector mass spectrometer equipped with a standard ESI source. Typically, a 5 μM protein solution in 100 mM

ammonium bicarbonate was continuously injected into the source at a flow rate of 5 μL/min. To avoid in-source oxidation of the protein ions, the spray needle potential was kept below 1.9 kVa. Acceleration voltage was kept at 5 kV, and the nominal resolution was set at 1000. All spectra were recorded by scanning the magnet at a rate of 5 s/decade. Typically, 80−180 scans were averaged for each spectrum to ensure an adequate signal-to-noise ratio. Protein denaturation was carried out by buffer exchanging the original samples into a solution whose pH was adjusted to 2.0 with glacial acetic acid. ESI MS measurements of acid-denatured protein samples were carried out using a QSTAR-XL (PE SCIEX, Framingham, MA) hybrid quadrupole-time-of-flight mass spectrometer equipped with a standard TurboSpray ESI source.

Affinity Measurements Using Surface Plasmon Resonance. A BIACORE 2000 biosensor system (Amersham Biosciences) was used to measure the affinities between the sTFR and hTF samples as described previously (*17*, *18*). Binding of injected hTF to sTFR immobilized on the sensor chip results in changes in SPR that are recorded in real time as resonance units (RU) (*45*, *46*). An oriented capture method was used to immobilize the purified sTFR samples on a CM5 sensor chip (Amersham Biosciences) by first immobilizing approximately 2200 RU of anti-penta-His antibody (Qiagen) by random amine coupling for all four flow cells. After the surface was blocked with 1 M ethanolamine, pH 8.0, approximately 300 RU of sTFR was immobilized per flow cell, with the exception of flow cell 1 which was used as a blank. In both experiments, the baseline for the N317D sTFR mutant decayed slightly during equilibration of the chip surface in running buffer, possibly accounting for a lower R_{max} relative to other flow cells, but was allowed to stabilize prior to analyte injection. Two separate CM5 chips were required to collect data for all five sTFR samples (BHK WT sTFR, insect cells WT sTFR, BHK N251D, BHK N317D, and BHK N727D). For each analyte (Fe_2 hTF, Fe_C hTF, and Mut-Fe_C hTF), a 2-fold dilution series of 10 concentrations preceded and followed by buffer blanks were injected over the flow cells at 70 μL/min at 25 °C in 50 mM Tris buffer, pH 7.4, 150 mM NaCl, and 0.005% P-20 surfactant. The chip surface was regenerated between sample injections with 30 μL of 1 M $MgCl_2$ in running buffer. Primary sensorgram data were preprocessed using the Scrubber software package (Biologic Software Pty.; http://www.biologic.com.au) and globally fitted to 2:1 or 1:1 models in Clamp XP, as previously described (*30*, *44*, *47*). Sensorgrams corresponding to the highest analyte concentration injections were dropped in the final fitting. The K_D values for the 1:1 models were statistically corrected with a factor of 0.5 such that they may be directly compared to the K_{D1} values for 2:1 models.

Complex Formation and Purification. To prepare Fe_C hTF/sTFR complexes for iron release studies, two different protocols were followed. In the first protocol, a molar excess of Fe_C hTF or Mut-Fe_C hTF was added to 1.0−1.5 mg of WT or mutant sTFR. Following reduction and filtration, the complex was loaded onto a Sephacryl S300HR 26/60 column, equilibrated, and chromatographed as described above. The fractions containing the complex (as confirmed by SDS−PAGE) were pooled and reduced in YM30 Centricon microconcentrators to a nominal concentration of 15 mg/mL. In the second protocol, Fe_C hTF/sTFR complexes were formed by the addition of a slight excess of sTFR and subsequent reduction using a microconcentrator.

Table 2: Production of Recombinant sTFR and the Glycosylation Mutants of sTFR from BHK Cells

recombinant sTFR	maximum production (mg/L) ± SD
N-His sTFR WT	34.4 ± 6.1, $n = 4$
N-His sTFR N251D	39.5 ± 8.5, $n = 4$
N-His sTFR N317D	15.5 ± 1.6, $n = 4$
N-His sTFR N727D	30.9 ± 0.9, $n = 2$

Kinetic Rate Studies. The rates of iron release from Mut-Fe_C hTF in complex with sTFR were determined at 25 °C using a QuantaMaster-6 fluorometer from Photon Technology International (PTI), with excitation at 280 nm and emission at 330 nm. A 3 mL cuvette containing 100 mM MES, pH 5.6, 300 mM KCl, and 4 mM EDTA in a volume of 1.8 mL (and a small stir bar to provide mixing) was placed in the fluorometer, and data collection was initiated to establish a baseline. Once equilibrated with respect to temperature, Mut-Fe_C hTF (∼500 nM) or the Mut-Fe_C hTF/sTFR complex (also 500 nM with respect to Mut-Fe_C hTF) was added by using a 25 μL Hamilton syringe through a port directly above the cuvette. The release of iron was monitored at 1 s intervals by measuring the increase in fluorescence. Data for a minimum of four samples were processed and analyzed using Origin 7.5 software and fitted to a single exponential linear equation ($Y = p_1e^{-x/p_2} + p_3 + p_4x$), which yielded R^2 values between 0.982 and 0.989.

For experiments with Fe_C hTF, iron release rates were determined using an Applied Photophysics (AP) SX.18MV stopped-flow spectrofluorometer fitted with a 20 μL observation cell with a 2 mm light path and a dead time of 1.1 ms. A monochromator was used for excitation at 280 nm, and the fluorescence emission was measured using a high-pass filter with a 320 nm cutoff. The temperature (25 °C) was kept constant using a circulating water bath. One syringe contained 375 nM (with respect to Fe_C hTF) complex in 1.0 mL of 300 mM KCl (pH ∼6.8). The other syringe contained 300 mM KCl, 200 mM MES, pH 5.6, and 8 mM EDTA. Kinetic traces were collected for 50 s intervals a total of six to eight times and averaged. At least three separate samples were averaged for each value reported. Data were analyzed using Origin 7.5 software fit best to a single exponential linear equation (as above); R^2 values varied from 0.996 to 0.999.

RESULTS

sTFR Production. WT sTFR (residues 121−760) and three single point mutants (N251D, N317D, and N727D) were expressed in BHK cells and secreted into the tissue culture medium. Each construct had four amino acids from the N-terminus of hTF and an N-His tag as well as a factor Xa cleavage site. As determined by a competitive immunoassay, the WT and mutant sTFR samples were expressed in this BHK system (Table 2). The results clearly show that production of WT sTFR and the N251D and N727D mutants is comparable, reaching a maximum of 30−40 mg/L, while the N317D mutant was approximately half of this value. Significantly, attempts to express a completely nonglycosylated sTFR construct (the N251D/N317D/N727D triple

Table 3: Determination of Masses by Electrospray Mass Spectrometry

recombinant sTFR[a]	post S300 column	monomer (dimer/2) (kDa)	dimer (kDa ± SD)	trimer[b] (kDa ± SD)
N-His sTFR (BHK)	peak	79.7	**159.4 ± 2.2**[c] **159.5 ± 2.8**	NO
	shoulder	80.1	**160.1 ± 2.7**	239.3 ± 2.9
N-His sTFR N251D	peak	77.1	**154.0 ± 1.4** **154.3 ± 1.8**	233.5 ± 3.9[d]
	shoulder	77.1	154.2 ± **1.6** 154.2 ± **1.2**	**233.9 ± 2.5** **233.6 ± 2.7**
N-His sTFR N317D	peak[e]	77.5	**154.4 ± 2.6** **155.5 ± 4.0**	234.1 ± 2.3[d] 235.3 ± 3.9
	shoulder	77.7	155.4 ± 2.8[d]	**235.0 ± 3.3**
N-His sTFR N727D	peak	78.1	**156.2 ± 2.9** **156.0 ± 2.6**	236.4 ± 3.8[d] 235.2 ± 2.8
	shoulder	NM[f]		
N-His sTFR (insect cells)	peak	83.6	**167.2 ± 3.0**	NO

[a] The calculated mass of the sTFR (residues 121−760) is 71726 Da, to which is added 440 Da for the V-P-D-K sequence, 823 Da for the hexa-His tag, and 456 Da for the factor Xa cleavage sequence for a total mass of 73445 Da. The difference is attributed to the carbohydrate (see Results and Discussion). [b] See text. We have determined that the trimer is made up of a dimer of TFR and a molecule of hTF. [c] The bold font indicates the major species present in each sample. [d] The precision of the mass determination on the indicated samples is ±100. All other samples have a precision of ±20. [e] In this sample, a species with a mass of 63470 Da was observed. [f] NM = not measured. NO = not observed.

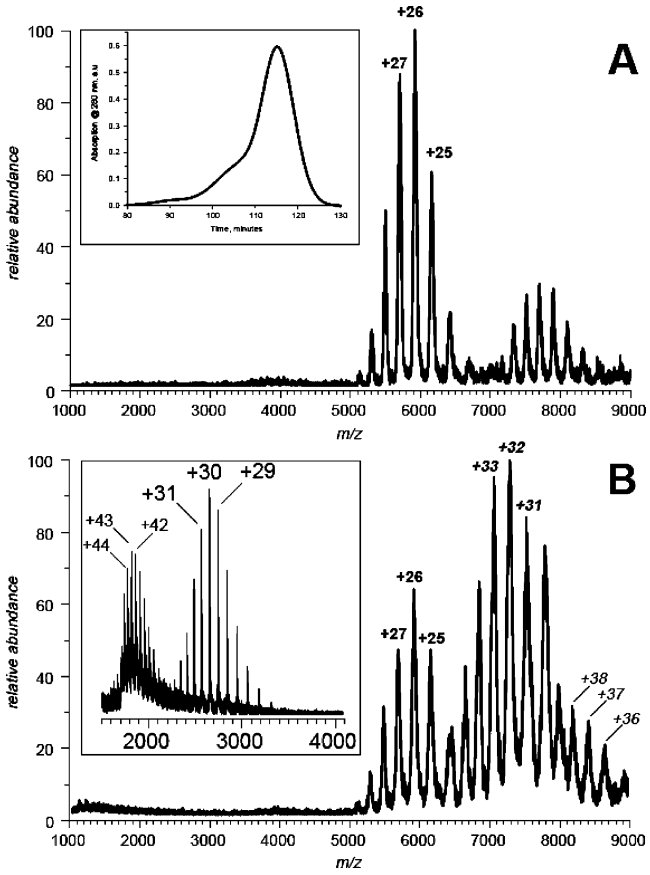

FIGURE 2: Electrospray ionization mass spectra of sTFR N251D size exclusion chromatography peaks: main peak (A) and shoulder (B). Both spectra were acquired under near-native conditions in solution (50 mM ammonium acetate). The elution profile is shown on the inset in panel A. Acid denaturation of the shoulder sample results in emergence of two distinct charge state distributions (inset in panel B), which correspond to the sTFR mutant and hTF (see text for more detail).

mutant) were unsuccessful. Both Western blot analysis and our competitive immunoassay confirmed the absence of any secreted sTFR. These results suggest either that glycosylation and secretion are intimately connected or that the secreted product is insoluble.

Following reduction and buffer exchange, the BHK cell medium containing recombinant sTFR was loaded onto a Ni-NTA column to capture the His-tagged constructs. After elution from the nickel column with 250 mM imidazole, final purification involved chromatography using an S300HR 26/60 gel filtration column. In each case, the main protein peak was preceded by a shoulder. Analysis of selected fractions on a 10% SDS−PAGE gel indicated that this shoulder contained a species with a higher molecular mass, as would be expected from the elution profile (see below). On the basis of the assay of the starting material, the yield of the recombinant sTFR constructs was ~60%; this yield is similar to our previously reported recoveries for recombinant hTF-NG (*40*).

Mass Spectrometry. The results of ESI MS analyses of various sTFR samples are summarized in Table 3. Since these experiments were carried out under near-native conditions, formation of multiple adducts resulted in significant broadening of the protein ion peaks in ESI mass spectra (see Figure 2 and Supporting Information) and resulted in rather modest mass measurement precision (ranging from 1.2 to 4.0 kDa for the major species, dimer). Nevertheless, the achieved precision is sufficient to confirm the predicted absence of glycosylation at a single site for each mutant when compared to the WT sTFR with glycans attached to all three sites. For each of the analyzed sTFR samples, the main peak from the S300HR column was always composed of a sTFR dimer, with a small amount of a tetrameric species also observed in all four sTFR preparations (Figure 2A). The presence of the tetrameric species in the mass spectra is not surprising, since such low-abundance oligomers are often observed in ESI MS under native conditions and are usually attributed to oligomerization stimulated by increased protein concentration in solution in the ESI interface (*48*). Although sTFR dimers were also observed in the shoulders of the N251D and N317D mutant peaks, a major species in each case had a significantly higher mass than the dimer but lower than the tetramers (Figure 2B). Such species were also observed in the WT sTFR shoulder peak and were only slightly less abundant than the sTFR dimer. Although the measured masses of these species are reasonably close to that of a putative sTFR homotrimer, the limited resolution and accuracy of measurements in the high *m*/*z* range make it impossible to assign the species solely on the basis of mass. For example, a putative heterotrimer composed of a sTFR dimer and a single TF molecule would have a mass within 2 kDa of the homotrimer. To establish the composition of this species unequivocally, the protein complex in question was denatured with acid, and its monomeric constituents were identified on the basis of their mass measurements in the low *m*/*z* region (Figure 2B inset). Since protein ions generated under denaturing conditions in solution do not form adducts as readily as those produced under native conditions,

Table 4: SPR Results for Binding of Fe_2 hTF, Fe_C hTF, and Mut-Fe_C hTF to WT sTFR and Three Glycosylation Mutants at pH 7.4[a]

transferrin	expt[b]	receptor	$K_{D1} \pm$ SE (nM)	$K_{D2} \pm$ SE (nM)
Fe_2 hTF	1	WT sTFR BHK	0.47 ± 0.003	15 ± 0.1
	1	sTFR N251D	0.51 ± 0.003	14 ± 0.1
	1	sTFR N317D	0.59 ± 0.01	19 ± 0.2
Fe_2 hTF	2	WT sTFR insect cells[c]	0.65 ± 0.01	10 ± 0.2
	2	sTFR N317D	0.57 ± 0.004	15 ± 0.1
	2	sTFRN727D	0.44 ± 0.003	13 ± 0.1
Fe_C hTF	1	WT sTFR BHK	22 ± 0.3	
	1	sTFR N251D	21 ± 0.3	
	1	sTFR N317D	31 ± 0.5	
Fe_C hTF	2	WT sTFR insect cells	28 ± 0.6	
	2	sTFR N317D	31 ± 0.5	
	2	sTFRN727D	21 ± 0.3	
Mut-Fe_C hTF	1	WT sTFR BHK	27 ± 0.3	
	1	sTFR N251D	31 ± 0.3	
	1	sTFR N317D	41 ± 0.6	
Mut-Fe_C hTF	2	WT sTFR insect cells	27 ± 0.6	
	2	sTFR N317D	31 ± 0.5	
	2	sTFRN727D	23 ± 0.3	

[a] Note that Fe_2 hTF binding is described by two dissociation constants and monoferric hTF binding is described by a single K_D. [b] The designations 1 and 2 refer to two different SPR chips needed to run all of the samples. [c] The WT sTFR in experiment 2 was expressed with a baculovirus/insect cell system.

significantly higher precision of mass measurement can be easily afforded. The mass spectrum of the acid-denatured protein sample reveals the presence of two distinct ionic species with masses of 79.6 ± 0.1 kDa (charge states +25 through +34) and 78.0 ± 0.1 kDa (charge states +37 through +45). Despite having similar masses, one of the protein species carries a significantly higher number of charges in the gas phase. This provides a rather clear indication that this protein remains more compact in denaturing solution than the other (*49*). This is an expected consequence of the presence of the large number of disulfide bonds in TF (19 total compared to only 2 in the sTFR), which prevent full unfolding of the TF polypeptide chain by imposing multiple conformational constraints. Taken together, measurements of the mass and the extent of multiple charging of the acid-denatured components of protein complexes giving rise to shoulder peaks on size-exclusion chromatograms clearly indicate that they are composed of both sTFR and TF monomers.

Binding of hTF to WT and Mutant sTFR Molecules. To compare the binding characteristics of each mutant sTFR to WT sTFR, equilibrium constants were calculated using an SPR assay to measure binding kinetics in real time (*17*, *30*). For these studies, the binding of three different analytes was measured: (1) glycosylated Fe_2 hTF, (2) Fe_C hTF, and (3) Mut-Fe_C hTF (selected for its slower rate of iron release; see below) (*44*). We observed that BHK-derived WT sTFR bound to glycosylated Fe_2 hTF with the same affinity as WT sTFR produced in the baculovirus/insect system (Table 4). Additionally, and as described previously, the Fe_2 hTF binding data were fit best with a bivalent model yielding two K_Ds, whereas Fe_C hTF and Mut-Fe_C hTF were consistent with a 1:1 model yielding a single K_D (*30*, *44*). The results indicate that the N251D and N727D sTFR mutants bind hTF

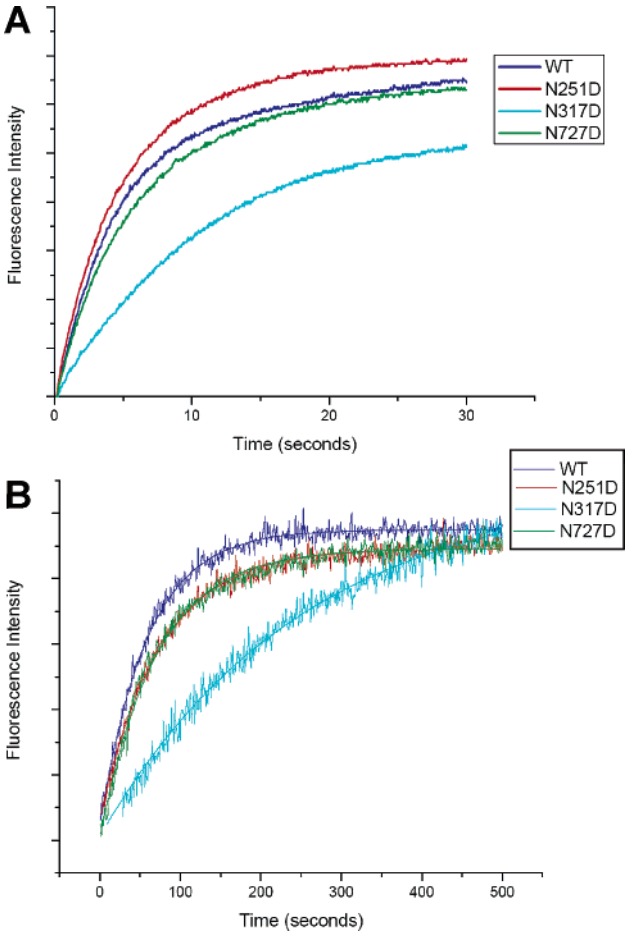

FIGURE 3: Progress curves for the rate of iron release from hTF species in a complex with WT sTFR and the three single glycosylation mutants of sTFR: (A) Fe_C hTF and (B) Mut-Fe_C hTF. The reduced noise observed in the fluorescent profiles of panel A is attributed to the greater sensitivity of the stopped-flow instrument and the averaging of six injections to produce the trace. Note that the time scales are very different in (A) and (B).

with nearly the same affinities as WT sTFR. In the case of the two Fe_C hTF constructs, the N317D sTFR mutant consistently bound with a lower affinity ($\sim 21.8 \pm 12.0\%$, $n = 4$). In contrast, the K_{D1} for Fe_2 hTF binding to the N317D mutant was within experimental error in both experiments. Two experiments were required to analyze all the samples, and the small differences between the two analytes were consistent with the experimental variability ascribed to differences in the individual chips.

Kinetic Studies. Iron release rates were determined by monitoring the increase in fluorescence as iron was released from Fe_C hTF in the presence and absence of sTFR. The fluorescent signal is ascribed to one or more of the five tryptophan residues in the C-lobe of hTF which become(s) unquenched and solvent-exposed as iron is released and the lobe opens (*44*, *50*). In previous studies, the fast rate of iron release from Fe_C hTF bound to sTFR yielded large standard deviations in the rate constants that were measured (*19*, *30*, *44*). In the current work, two strategies were employed to measure the rates with greater precision. In one approach, a stopped-flow instrument from Applied Photophysics was used to acquire the data for the Fe_C hTF/sTFR complexes at pH 5.6. Kinetic curves for each complex are shown in Figure 3A.

Table 5: Kinetics of Iron Release from hTF Mutants with and without sTFR[a]

proteins[b]	k_{obs} ($s^{-1} \times 10^3$) ± SD	instrument[c]
Fe_C hTF control	3.4 ± 0.1	Cary
Fe_C hTF + N-His sTFR WT insect cells	262 ± 44	PTI
Fe_C hTF + N-His sTFR WT BHK	249 ± 68	PTI
Fe_C hTF + N-His sTFR WT	238 ± 22	AP
Fe_C hTF + N-His sTFR N251D	204 ± 9	AP
Fe_C hTF + N-His sTFR N317D	90 ± 10	AP
Fe_C hTF + N-His sTFR N727D	175 ± 6	AP
Mut-Fe_C hTF[d]	0.087 ± 0.017	Cary
Mut-Fe_C hTF + N-His sTFR WT[d]	18 ± 1	PTI
Mut-Fe_C hTF + N-His sTFR N251D	16 ± 0.1	PTI
Mut-Fe_C hTF + N-His sTFR N317D	8 ± 1	PTI
Mut-Fe_C hTF + N-His sTFR N727D	17 ± 0.1	PTI

[a] Iron release from hTF mutants was determined at 25 °C and pH 5.6 (100 mM MES, 4 mM EDTA, 300 mM KCl). [b] The control is N-His Y95F/Y188F hTF-NG. All constructs are in this background. [c] Measurements were carried out as described in Materials and Methods on a Varian Cary 100 dual beam spectrophotometer, a Photon Technology International QuantaMaster (PTI) spectrofluorometer, or an Applied Photophysics (AP) SX.18MV stopped-flow spectrofluorometer as indicated above. [d] The mutant is N-His Y95F/Y188F/R632N/D634N hTF-NG, and the release rate for the mutant alone has been previously reported (*44*). In addition, the rate for the mutant in the presence of the sTFR from the insect cells was reported as 25.5 ± 0.9 $s^{-1} \times 10^{-3}$, $n = 3$ (*44*).

A second approach to simplify comparisons involved the use of a mutant (designated Mut-Fe_C hTF) with a slower rate of release (30-fold slower in the absence of TFR and 9-fold slower in the presence of TFR) when compared to Fe_C hTF (*44*). This mutant was originally designed to mimic the composition of a triad of residues found in the C-lobe of lactoferrin which is well-known to have slower iron release rates than ovotransferrin or hTF. Typical release curves from the Mut-Fe_C hTF/sTFR complexes are shown in Figure 3B. A summary of the kinetic rate constants for each sTFR bound to Fe_C hTF and Mut-Fe_C hTF is presented in Table 5. The results clearly show that the N317D sTFR mutant has a 2−3-fold slower release rate than the WT sTFR and the N251D or N727D sTFR mutants.

Since our earlier studies (*30*, *44*) utilized sTFR from baculovirus/insect cells, we wanted to verify the assumption that the two recombinant forms of the WT sTFR are functionally equivalent. Because the amino acid sequence of each WT sTFR differs only by the presence of four extra amino acids (with a mass of 440 Da) preceding the His tag in the BHK-derived sTFR, most of the difference in mass resides in the composition of the carbohydrate. As shown in Table 3, analysis by mass spectrometry reveals that the baculovirus/insect cell derived sTFR is slightly larger (see Discussion). Nevertheless, the SPR data indicate that the binding of Fe_2 hTF to the two recombinant sTFR samples is identical (Table 4). Additionally, iron release rates for Fe_C hTF in a complex with either the BHK or insect cell derived sTFR are the same within experimental error (Table 5).

DISCUSSION

By transfecting BHK cells with a mutant in which the three asparagine linkage sites were converted to aspartic acid, we hoped to express a recombinant form of sTFR that lacked glycosylation. We anticipated that production of a nonglycosylated sTFR would provide a homogeneous preparation for use in mass spectroscopy studies and might aid in crystallization trials. Unfortunately, no nonglycosylated sTFR was secreted into the tissue culture medium of the BHK cells as indicated by an immunoassay and further confirmed by Western blot analysis using a probe for the His tag. This finding differs from expression of hTF, in which glycosylation plays no role in either expression or function (*51*), but is consistent with a report of the failure of the nonglycosylated mutant to reach the cell surface in TFR-deficient CHO cells (*10*). The inability to express the completely nonglycosylated sTFR led us to produce the single sTFR glycosylation mutants individually to facilitate an assessment of the role of each glycosylation site in the expression and function of the sTFR. In our laboratory, the secreted His-tagged sTFR from the baculovirus/insect cell medium obtained from the expression facility at The California Institute of Technology was purified with a final yield of 13.6 ± 4.4 mg/L, $n = 8$. In the present work, we find that the yield of sTFR from the BHK expression system is comparable, 11.6 ± 4.3 mg/L, $n = 4$. In each case, the yield of functional sTFR is considerably higher than amounts reported either from the CHO cell system (∼2 mg/L) (*11*) or from placental preparations (2−6 mg of full-length TFR per placenta) (*52*, *53*).

As previously noted (*11*, *54*, *55*), even in the absence of the disulfide linkages in the stalk region, the WT and each of the mutant sTFR constructs form dimers in solution as clearly shown by their behavior during gel filtration chromatography and by mass spectrometry analysis (Table 3). Although it is clear that glycosylation of two of the three sites allows expression, it is unclear whether it might be possible to express a sTFR with a single glycan. Our results make it tempting to speculate that only the carbohydrate at position 317 may be crucial to the production of functional sTFR.

Determining the exact composition of the carbohydrate at each site is extremely challenging because although BHK cells and insect cells attach carbohydrate at the consensus sequences, the composition of the attached carbohydrate is usually variable in both a cell type- and species-dependent manner (ref *51* and references cited therein). Interestingly, in naturally occurring TFR, the complexity of the carbohydrate appears to be specific to the position of the Asn residues in the sequence (*32*). Thus, it has been reported that human TFR isolated from placenta and TFR expressed in mouse NIH-3T3 cells show similar patterns (*32*); the Asn251 site featured a complex triantennary, trisialylated carbohydrate with a fucose core (3009 Da), the Asn317 site had a sialylated hybrid oligosaccharide (1874 Da), and Asn727 had a high mannose type oligosaccharide (1866 Da). Our measurements do not allow such a detailed determination of the carbohydrate composition at each site.

Identification of a "trimer" by mass spectrometry analysis is attributed to the presence of a TFR dimer with a single molecule of hTF bound. At the resolution of the analysis the difference in mass between a TFR monomer and a molecule of hTF is indistinguishable. Using acid denaturation and analysis in the low *m*/*z* region, we were able to make the distinction unequivocally. As previously reported (*39*), hTF is present in the serum substitute Ultroser G at a concentration of ∼2−4 mg/L. Due to the high affinity of

the hTF/TFR interaction, it is extremely likely that any hTF in the tissue culture medium that acquires iron would bind to the recombinant TFR. Likewise, the complex would be expected to elute from the gel filtration column as a higher molecular weight "shoulder".

Elimination of the carbohydrate at position 251 has little or no effect on the expression, dimerization, complex formation, and release of iron from TF compared to WT. Previous work showed that glycosylation at position 251 is necessary for protection against proteolysis (*34*), although no proteolysis was observed in another study (*36*). The carbohydrate at position 251 was not involved in ligand binding and/or dimerization of the TFR in vivo (*34*). Likewise, we observed no interference with complex formation or dimerization of the N251D mutant, and obviously, protection from proteolysis is not relevant in expression of the secreted soluble portion of the TFR.

In our studies, the N317D sTFR mutant expressed poorly and was more difficult to purify. We note that this mutant appears to be less soluble and/or is possibly more prone to aggregation. In the case of the two Fe_C hTF samples, the absence of carbohydrate at this position causes a small difference of ~20% in the binding affinity measured at pH 7.4 although, interestingly, no significant difference was found for binding of Fe_2 hTF to this mutant (Table 4). Examination of the crystal structure of sTFR (Figure 1) reveals that residue 317 from one monomer is within 4 Å of W641 and F760 on the other monomer. As described in the introduction, these two residues comprise a hydrophobic patch on the TFR that is involved in the binding of hTF. This patch appears to be responsible for stabilization of apo-hTF at acidic pH (*30*). The absence of carbohydrate at position 317 has a small impact on the affinity for Fe_C hTF at pH 7.4. Additionally, the rate of iron release at pH 5.6 is 2−3-fold slower. These results imply that the carbohydrate at this position helps to attain and/or stabilize the conformation of the sTFR in a pH-dependent manner. Consistent with this idea is the observation that the affinity of Fe_2 hTF for the N317D sTFR is the same as that found for WT sTFR and the other mutants (Table 4). Likewise, the change in affinity for the hydrophobic patch double mutant was only observed at pH 6.3 and 5.6. Thus, the finding of equal affinity for Fe_2 hTF at neutral pH is consistent, and the N317D glycosylation may have a role in stabilizing the bound apo-hTF at low pH.

Previous studies indicated that the carbohydrate at position 727 is important in proper folding of the TFR and crucial to transport of the TFR to the plasma membrane (*33*, *36*). Obviously, production of the soluble TFR does not require the intracellular trafficking function. In addition, the current work does not suggest that the sTFR is improperly folded since the mutant is expressed at a concentration that is equivalent to the control (Table 2), binds equally well to the various hTF constructs (Table 4), and yields a similar acceleration in the rate of iron release from the C-lobe of hTF (Table 5). Therefore, and within the context of the soluble TFR, the absence of carbohydrate at position 727 has no impact on any of the measured criteria.

In summary, we present data that demonstrate the importance of glycosylation in the expression of the sTFR; no sTFR is expressed when the three sites are mutated to prevent glycosylation. We show that, in contrast to expression of full-length TFR, only the carbohydrate at position 317 has a significant effect on the expression and iron release rates of the soluble form of the TFR. Additionally, we have shown that the stopped-flow spectrofluorometer is able to capture iron release rates with greater precision and sensitivity than previously used methods.

ACKNOWLEDGMENT

We thank Dr. Caroline A. Enns for the full-length human TFR cDNA clone. We also thank Julia R. Larouche and Caroline George (SURE Program) for able technical assistance. We are very grateful to the College of Medicine at the University of Vermont for a grant to purchase the Applied Photophysics (AP) SX.18MV stopped-flow spectrofluorometer and to Dr. Iwona A. Buskiewicz for showing us how to use it.

SUPPORTING INFORMATION AVAILABLE

One figure displaying zoomed regions of ESI mass spectra showing ionic signals of sTFR species. This material is available free of charge via the Internet at http://pubs.acs.org.

REFERENCES

1. MacGillivray, R. T. A., Moore, S. A., Chen, J., Anderson, B. F., Baker, H., Luo, Y. G., Bewley, M., Smith, C. A., Murphy, M. E., Wang, Y., Mason, A. B., Woodworth, R. C., Brayer, G. D., and Baker, E. N. (1998) Two high-resolution crystal structures of the recombinant N-lobe of human transferrin reveal a structural change implicated in iron release, *Biochemistry 37*, 7919−7928.
2. Young, S. P., Bomford, A., and Williams, R. (1984) The effect of the iron saturation of transferrin on its binding and uptake by rabbit reticulocytes, *Biochem. J. 219*, 505−510.
3. Mason, A. B., Halbrooks, P. J., James, N. G., Connolly, S. A., Larouche, J. R., Smith, V. C., MacGillivray, R. T. A., and Chasteen, N. D. (2005) Mutational analysis of C-lobe ligands of human serum transferrin: insights into the mechanism of iron release, *Biochemistry 44*, 8013−8021.
4. Aisen, P. (2004) Transferrin receptor 1, *Int. J. Biochem. Cell Biol. 36*, 2137−2143.
5. Rybak, S. L., and Murphy, R. F. (1998) Primary cell cultures from murine kidney and heart differ in endosomal pH, *J. Cell. Physiol. 176*, 216−222.
6. Ohgami, R. S., Campagna, D. R., Greer, E. L., Antiochos, B., McDonald, A., Chen, J., Sharp, J. J., Fujiwara, Y., Barker, J. E., and Fleming, M. D. (2005) Identification of a ferrireductase required for efficient transferrin-dependent iron uptake in erythroid cells, *Nat. Genet. 37*, 1264−1269.
7. Gunshin, H., and Hediger, M. A. (2002) The divalent metal-ion transporter (DCT1/DMT1/Nramp2), in *Molecular and Cellular Iron Transport* (Templeton, D. M., Ed.) pp 155−173, Marcel Dekker, New York.
8. Teeters, C. L., Lodish, H. F., Ciechanover, A., and Wallace, B. A. (1986) Transferrin and apotransferrin: pH-dependent conformational changes associated with receptor-mediated uptake, *Ann. N.Y. Acad. Sci. 463*, 403−407.
9. Kawabata, H., Yang, R., Hirama, T., Vuong, P. T., Kawano, S., Gombart, A. F., and Koeffler H. P. (1999) Molecular cloning of transferrin receptor 2. A new member of the transferrin receptor-like family, *J. Biol. Chem. 274*, 20826−20832.
10. Yang, B., Hoe, M. H., Black, P., and Hunt, R. C. (1993) Role of oligosaccharides in the processing and function of human transferrin receptors. Effect of the loss of the three *N*-glycosyl oligosaccharides individually or together, *J. Biol. Chem. 268*, 7435−7441.
11. Lawrence, C. M., Ray, S., Babyonyshev, M., Galluser, R., Borhani, D. W., and Harrison, S. C. (1999) Crystal structure of the ectodomain of human transferrin receptor, *Science 286*, 779−782.

12. Enns, C. A., Clinton, E. M., Reckhow, C. L., Root, B. J., Do, S.-I., and Cook, C. (1991) Acquisition of the functional properties of the transferrin receptor during its biosynthesis, *J. Biol. Chem. 266*, 13272−13277.
13. McClelland, A., Kuhn, L. C., and Ruddle, F. H. (1984) The human transferrin receptor gene: genomic organization, and the complete primary structure of the receptor deduced from a cDNA sequence, *Cell 39*, 267−274.
14. Schneider, C., Owen, M. J., Banville, D., and Williams, J. G. (1984) Primary structure of human transferrin receptor deduced from the mRNA sequence, *Nature 311*, 675−678.
15. Kuhn, L. C., McClelland, A., and Ruddle, F. H. (1984) Gene transfer, expression, and molecular cloning of the human transferrin receptor gene, *Cell 37*, 95−103.
16. Lebrön, J. A., and Bjorkman, P. J. (1999) The transferrin receptor binding site on HFE, the class I MHC-related protein mutated in hereditary hemochromatosis, *J. Mol. Biol. 289*, 1109−1118.
17. Giannetti, A. M., Snow, P. M., Zak, O., and Bjorkman, P. J. (2003) Mechanism for multiple ligand recognition by the human transferrin receptor, *PLoS Biol. 1*, 341−350.
18. West, A. P., Jr., Giannetti, A. M., Herr, A. B., Bennett, M. J., Nangiana, J. S., Pierce, J. R., Weiner, L. P., Snow, P. M., and Bjorkman, P. J. (2001) Mutational analysis of the transferrin receptor reveals overlapping HFE and transferrin binding sites, *J. Mol. Biol. 313*, 385−397.
19. Zak, O., and Aisen, P. (2003) Iron release from transferrin, its C-lobe, and their complexes with transferrin receptor: Presence of N-lobe accelerates release from C-lobe at endosomal pH, *Biochemistry 42*, 12330−12334.
20. Enns, C. A. (2001) Pumping iron: the strange partnership of the hemochromatosis protein, a class I MHC homolog, with the transferrin receptor, *Traffic 2*, 167−174.
21. Giannetti, A. M., and Bjorkman, P. J. (2004) HFE and transferrin directly compete for transferrin receptor in solution and at the cell surface, *J. Biol. Chem. 279*, 25866−25875.
22. Bennett, M. J., Lebrón, J. A., and Bjorkman, P. J. (2000) Crystal structure of the hereditary haemochromatosis protein HFE complexed with transferrin receptor, *Nature 403*, 46−53.
23. Dubljevic, V., Sali, A., and Goding, J. W. (1999) A Conserved RGD (Arg-Gly-Asp) motif in the transferrin receptor is required for binding to transferrin, *Biochem. J. 341*, 11−14.
24. Bali, P. K., Zak, O., and Aisen, P. (1991) A new role for the transferrin receptor in the release of iron from transferrin, *Biochemistry 30*, 324−328.
25. Bali, P. K., and Aisen, P. (1991) Receptor-modulated iron release from transferrin: Differential effects on N- and C-terminal sites, *Biochemistry 30*, 9947−9952.
26. Bali, P. K., and Aisen, P. (1992) Receptor-induced switch in site−site cooperativity during iron release by transferrin, *Biochemistry 31*, 3963−3967.
27. Aisen, P. (1992) Entry of iron into cells: a new role for the transferrin receptor in modulating iron release from transferrin, *Ann. Neurol. 32* (Suppl.), S62−S68.
28. Liu, R. T., Guan, J. Q., Zak, O., Aisen, P., and Chance, M. R. (2003) Structural reorganization of the transferrin C-lobe and transferrin receptor upon complex formation: The C-lobe binds to the receptor helical domain, *Biochemistry 42*, 12447−12454.
29. Cheng, Y., Zak, O., Aisen, P., Harrison, S. C., and Walz, T. (2004) Structure of the human transferrin receptor-transferrin complex, *Cell 116*, 565−576.
30. Giannetti, A. M., Halbrooks, P. J., Mason, A. B., Vogt, T. M., Enns, C. A., and Bjorkman, P. J. (2005) The molecular mechanism for receptor-stimulated iron release from the plasma iron transport protein transferrin, *Structure 13*, 1613−1623.
31. Reckhow, C. L., and Enns, C. A. (1988) Characterization of the transferrin receptor in tunicamycin-treated A431 cells, *J. Biol. Chem. 263*, 7297−7301.
32. Hayes, G. R., Williams, A. M., Lucas, J. J., and Enns, C. A. (1997) Structure of human transferrin receptor oligosaccharides: Conservation of site-specific processing, *Biochemistry 36*, 5276−5284.
33. Williams, A. M., and Enns, C. A. (1991) A mutated transferrin receptor lacking asparagine-linked glycosylation sites shows reduced functionality and an association with binding immunoglobulin protein, *J. Biol. Chem. 266*, 17648−17654.
34. Hoe, M. H., and Hunt, R. C. (1992) Loss of one asparagine-linked oligosaccharide from human transferrin receptors results in specific cleavage and association with the endoplasmic reticulum, *J. Biol. Chem. 267*, 4916−4923.
35. Hunt, R. C., Riegler, R., and Davis, A. A. (1989) Changes in glycosylation alter the affinity of the human transferrin receptor for its ligand, *J. Biol. Chem. 264*, 9643−9648.
36. Williams, A. M., and Enns, C. A. (1993) A region of the C-terminal portion of the human transferrin receptor contains an asparagine-linked glycosylation site critical for receptor structure and function, *J. Biol. Chem. 268*, 12780−12786.
37. Wang, C., Eufemi, M., Turano, C., and Giartosio, A. (1996) Influence of the carbohydrate moiety on the stability of glycoproteins, *Biochemistry 35*, 7299−7307.
38. Rudd, P. M., Joao, H. C., Coghill, E., Fiten, P., Saunders, M. R., Opdenakker, G., and Dwek, R. A. (1994) Glycoforms modify the dynamic stability and functional activity of an enzyme, *Biochemistry 33*, 17−22.
39. Mason, A. B., He, Q.-Y., Adams, T. E., Gumerov, D. R., Kaltashov, I. A., Nguyen, V., and MacGillivray, R. T. A. (2001) Expression, purification, and characterization of recombinant nonglycosylated human serum transferrin containing a C-terminal hexahistidine tag, *Protein Expression Purif. 23*, 142−150.
40. Mason, A. B., Halbrooks, P. J., Larouche, J. R., Briggs, S. K., Moffett, M. L., Ramsey, J. E., Connolly, S. A., Smith, V. C., and MacGillivray, R. T. A. (2004) Expression, purification, and characterization of authentic monoferric and apo-human serum transferrins, *Protein Expression Purif. 36*, 318−326.
41. Lebrón, J. A., Bennett, M. J., Vaughn, D. E., Chirino, A. J., Snow, P. M., Mintier, G. A., Feder, J. N., and Bjorkman, P. J. (1998) Crystal structure of the hemochromatosis protein HFE and characterization of its interaction with transferrin receptor, *Cell 93*, 111−123.
42. Mason, A. B., Funk, W. D., MacGillivray, R. T. A., and Woodworth, R. C. (1991) Efficient production and isolation of recombinant amino-terminal half-molecule of human serum transferrin from baby hamster kidney cells, *Protein Expression Purif. 2*, 214−220.
43. Pace, C. N., Vajdos, F., Fee, L., Grimsley, G., and Gray, T. (1995) How to measure and predict the molar absorption coefficient of a protein, *Protein Sci. 4*, 2411−2423.
44. Halbrooks, P. J., Giannetti, A. M., Klein, J. S., Bjorkman, P. J., Larouche, J. R., Smith, V. C., MacGillivray, R. T. A., Everse, S. J., and Mason, A. B. (2005) Composition of pH sensitive triad in C-lobe of human serum transferrin. Comparison to sequences of ovotransferrin and lactoferrin provides insight into functional differences in iron release, *Biochemistry 44*, 15451−15460.
45. Fagerstam, L. G., Frostell-Karlsson, A., Karlsson, R., Persson, B., and Ronnberg, I. (1992) Biospecific interaction analysis using surface plasmon resonance detection applied to kinetic, binding site and concentration analysis, *J. Chromatogr. 597*, 397−410.
46. Malmqvist, M. (1993) Biospecific interaction analysis using biosensor technology, *Nature 361*, 186−187.
47. Myszka, D. G., and Morton, T. A. (1998) CLAMP: a biosensor kinetic data analysis program, *Trends Biochem. Sci. 23*, 149−150.
48. Peschke, M., Verkerk, U. H., and Kebarle, P. (2004) Features of the ESI mechanism that affect the observation of multiply charged noncovalent protein complexes and the determination of the association constant by the titration method, *J. Am. Soc. Mass Spectrom. 15*, 1424−1434.
49. Kaltashov, I. A., and Eyles, S. J. (2002) Studies of biomolecular conformations and conformational dynamic by mass spectrometry, *Mass Spectrom. Rev. 21*, 37−71.
50. Lehrer, S. S. (1969) Fluorescence and absorption studies of the binding of copper and iron to transferrin, *J. Biol. Chem. 244*, 3613−3617.
51. Mason, A. B., Miller, M. K., Funk, W. D., Banfield, D. K., Savage, K. J., Oliver, R. W. A., Green, B. N., MacGillivray, R. T. A., and Woodworth, R. C. (1993) Expression of glycosylated and nonglycosylated human transferrin in mammalian cells. Characterization of the recombinant proteins with comparison to three commercially available transferrins, *Biochemistry 32*, 5472−5479.
52. Turkewitz, A. P., Amatruda, J. F., Borhani, D., Harrison, S. C., and Schwartz, A. L. (1988) A high yield purification of the human transferrin receptor and properties of its major extracellular fragment, *J. Biol. Chem. 263*, 8318−8325.

53. Hemadi, M., Kahn, P. H., Miquel, G., and Hage Chahine, J. M. (2004) Transferrin's mechanism of interaction with receptor 1, *Biochemistry 43*, 1736−1745.
54. Borhani, D. W., and Harrison, S. C. (1991) Crystallization and X-ray diffraction studies of a soluble form of the human transferrin receptor, *J. Mol. Biol. 218*, 685−689.
55. Fuchs, H., Lücken, U., Tauber, R., Engel, A., and Gessner, R. (1998) Structural model of phospholipid-reconstituted human transferrin receptor derived by electron microscopy, *Structure 6*, 1235−1243.

BI0600695